Mechanochemical synthesis and consolidation of nanostructured cerium hexaboride

Duygu Ağaoğulları[1,*], Özge Balcı[2], Nazlı Akçamlı[3], Challapalli Suryanarayana[4], İsmail Duman[1], Mustafa Lütfi Öveçoğlu[1]

[1]*Istanbul Technical University, Faculty of Chemical and Metallurgical Engineering, Department of Metallurgical and Materials Engineering, Particulate Materials Laboratories, 34469 Maslak, Istanbul, Turkey*
[2]*Koç University, Department of Chemistry, Rumelifeneri Yolu, 34450 Sarıyer, İstanbul, Turkey*
[3]*Bursa Technical University, Faculty of Natural Sciences, Architecture and Engineering, Department of Metallurgical and Materials Engineering, Osmangazi, 16190 Bursa, Turkey*
[4]*Department of Mechanical and Aerospace Engineering, University of Central Florida, Orlando, FL 32816-2450, USA*

Abstract

This study reports on the mechanochemical synthesis (MCS) and consolidation of nanostructured CeB_6 powders of high purity. CeB_6 powders were prepared via MCS by milling CeO_2, B_2O_3 and Mg powders in a high-energy ball mill for different milling times. The effects of milling time on the formation, microstructure and thermal behaviour of the synthesized powders were investigated and the optimum MCS duration was determined. Purified powders were obtained after HCl leaching by removing MgO by-product. The prepared powders were characterized by a number of techniques including X-ray diffraction, stereomicroscopy, scanning and transmission electron microscopy coupled with energy dispersive spectrometry, differential scanning calorimetry, atomic absorption spectrometry, particle size analysis, surface area analysis and vibrating sample magnetometry. The high-purity CeB_6 powders having an average particle size of 86 nm were consolidated by cold-pressing followed by pressureless sintering at 1700 °C for 5 h. The bulk CeB_6 specimen was investigated for its microstructure, density, electrical resistivity, surface roughness and some mechanical properties (micro-hardness and wear behaviour). The relative density, electrical resistivity, microhardness and wear rate of the bulk CeB_6 were determined as 95.2% TD, 57.50 μΩ·cm, 11.65 GPa and 1.46×10^{-4} mm³/N·m, respectively.

Keywords: borides, mechanochemical synthesis, sintering, microstructure, mechanical properties

I. Introduction

Cerium hexaboride (CeB_6), a refractory ceramic material, has attracted significant interest in recent years among transition metal borides and rare-earth metal borides. It crystallizes in a CsCl-type structure with a space group of *Pm3m* symmetry, where the cerium ions occupy the Cs sites and octahedral B_6 molecules are located at the Cl sites [1]. CeB_6 exhibits low density (~4.79 g/cm³), high melting temperature (~2550 °C), high hardness (~2530 HV), high chemical and thermal stability, low electrical resistivity (~30 μΩ·cm), high

thermal conductivity (~34 W/m·K), low electronic work function (~2.5 eV), low coefficient of thermal expansion (~7.4×10⁻⁶ K⁻¹) and high neutron absorbability [1–12]. Among the known hexaborides, CeB_6 has an interesting physical property of dense Kondo behaviour [1,13]. The combination of these properties enables CeB_6 to be used in special applications, such as materials for wave-absorption, cathode emission and nuclear fields [14]. CeB_6 is considered an excellent field electron emitter source for various devices with its low work function [3,7]. It is also used in high energy optical systems and in sensors for high-resolution detectors due to its long service life time and low volatility at high temperatures [2]. CeB_6 has also attracted considerable at-

*Corresponding author: tel: +90 212 285 68 58,
e-mail: bozkurtdu@itu.edu.tr

tention because it shows several interesting phases in the presence of magnetic field and temperature such as antiferro-quadrupolar ordered phase and antiferromagnetic ordered phase [13,15].

Traditionally, CeB_6 is synthesized by high temperature reaction processes such as direct solid-phase reaction of cerium or its oxides with elemental boron and carbothermal synthesis using carbon and boron carbide [7,13,14,16–18]. However, the disadvantages of these methods, such as high content of carbon or high processing temperatures, limit the possibility of preparing CeB_6 powders with high purity and fine particle sizes [14]. In the literature, CeB_6 was produced by borothermal reduction of CeO_2 with a boron source, under formation of volatile boron suboxides at 1200–1800 °C in vacuum [17]. Similarly, CeB_6 was prepared by the reaction of CeO_2 with B_4C at 1600 °C after 60 min under vacuum and it was stated that 0.02 wt.% of C remained in the product due to the formation of gaseous reaction products [18]. CeB_6 was also prepared from its oxide by reacting with boron (10 wt.% stoichiometric excess) and carbon at 1500 °C for 15 h under Ar atmosphere [19].

Recently, CeB_6 powders were prepared via different synthesis techniques, such as self-propagating high temperature synthesis (SHS - also known as combustion synthesis), mechanochemical, electrochemical and gas phase synthesis methods. Accordingly, nanoscale CeB_6 powders were prepared by SHS using CeO_2, B_2O_3 and Mg as raw materials [14,20]. After leaching of the SHS products, CeB_6 powders were obtained with purity higher than 99% and an average particle size of 30–70 nm [14]. Akgun *et al.* [21] reported the mechanochemical and combustion synthesis of CeB_6 starting from CeO_2, B_2O_3 and Mg powder mixtures. It was stated that after the leaching processes, the respective reaction yields were 68.6% and 84.4%, and average particle sizes were 290 and 240 nm for combustion and mechanochemical synthesis methods, respectively [21]. Furthermore, CeB_6 nanowires with a diameter of around 20–100 nm were synthesized by self-catalyst metal-gas reaction method at 1125 °C on a Si substrate using Ce powders and $BCl_3/H_2/Ar$ gas mixtures [7]. Furthermore, several investigations relate the synthesis of CeB_6 films or coatings and their field emission properties [13,22,23]. Bluish-violet CeB_6 ranging in size between 4 and 40 μm was produced at 1250 and 1300 °C for 2 h through reactions of $CeCl_3$ with circulating H_2/Ar gas mixture (after dehydration of $CeCl_3 \cdot 7H_2O$ at 100 °C for 24 h under a reduced pressure of 10^{-3} Pa) or CeF_3 with amorphous or crystalline boron in the presence and absence of Al reducing agent, using conventional apparatus such as graphite crucible or alumina boat placed into a tubular furnace [24,25]. Additionally, electrochemical synthesis (at 900 °C) was performed to obtain CeB_6 crystals by using the molten salt technique from the electrolyte consisting of $LiCl/Li_2B_4O_7/CeCl_3$ [11] and $LiF/B_2O_3/CeCl_3$ [12] raw materials.

It has been reported that bulk rare-earth hexaborides with high density cannot be prepared easily via conventional hot-pressing method due to their high plastic yield stress [26]. Although fully dense rare-earth bulk CeB_6 can be prepared by sintering, the process of sintering the powders has not been comprehensively investigated in the literature. Recently, ball milled CeB_6 nanopowders were fully densified at 1000–1550 °C and a pressure of 50 MPa by using spark plasma sintering (SPS) method [26]. Polycrystalline bulk CeB_6 cathodes were fabricated via SPS method using the mixed powders of nano-CeH_x and micron-sized boron. High density CeB_6 sintered body was obtained at 1500 °C under a pressure of 50 MPa and holding time of 5 min [27].

Apart from the above-mentioned synthesis techniques, mechanochemistry is a novel, simple and room-temperature process which enables control of the product microstructure (phase, shape, size, etc.) and obtaining homogeneous materials [28]. In the present study, nanostructured CeB_6 powders were fabricated via mechanochemical route using low-cost raw materials of CeO_2, B_2O_3 and Mg powders and simple equipment. The effect of milling duration on the obtained phases was investigated as a process parameter in detail. A purification treatment was applied after the synthesis process to achieve high-purity CeB_6 powders. Consolidation of the synthesized powders was conducted by pressureless sintering and the bulk CeB_6 specimen was studied for its microstructural and some physical and mechanical properties. We report here the first study of the synthesis and consolidation of homogeneous nanocrystalline bulk CeB_6.

II. Materials and methods

2.1. Raw materials and precursor preparation

CeO_2 (ABCR™, 99.99% pure), B_2O_3 (ETI Mine, 98% pure) and Mg powders (MME, 99.7% pure) were used as the sources of cerium and boron, and reducing agent, respectively. The average particle sizes of the CeO_2, B_2O_3 and Mg starting powders were measured by using a Malvern™ Mastersizer 2000 particle size analyser and determined as 9.5 μm, 466.9 μm and 142.7 μm, respectively.

Stoichiometry for the synthesis of CeB_6 from the CeO_2, B_2O_3 and Mg powders is given by the reduction reaction in Eq. 1. The stoichiometric amounts of the initial reactants CeO_2 : B_2O_3 : Mg were 1.593 : 1.933 : 2.474 g for powders as per Eq. 1. Thus, the total powder batches of 6 g were weighed under Ar atmosphere (Linde™, 99.999% pure) in a Plaslabs™ glove box.

$$CeO_2 + 3B_2O_3 + 11Mg \longrightarrow CeB_6 + 11MgO \quad (1)$$
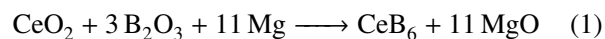
Powder batches were mixed in a WAB™ T2C Turbula blender for 1 h with the aim of homogenization and named as-blended powders hereafter.

2.2. Mechanochemical synthesis and purification

Mechanochemical synthesis (MCS) was conducted by milling the as-blended powders in a high-energy Spex™ 8000D Mixer/Mill at 1200 rpm for different durations up to 5 h. The required energy needed to trigger the reaction was supplied by the high-energy collisions, induced into powder particles via mechanical deformation. The ball-to-powder weight ratio was kept constant at 10 : 1. Hardened steel vial (50 ml) and hardened steel balls (6 mm diameter) were used as milling media. Milling vials were sealed under Ar atmosphere in the glove-box.

After MCS, selective acid leaching was applied for removal of MgO by-product with 4 M HCl solution under effect of ultrasonic stirring and heating using a Bandelin Sonorex™ RK-100H ultrasonic bath. The leaching treatment was conducted at 80 °C for 15 min with a solid-to-liquid ratio of 1 g/10 cm³. The residue was then separated from the leaching solution by repeated centrifugation (Hettich™ Rotofix 32 A, 3500 rpm, 30 min), decantation and rinsing steps. The residue was dried in an FN 500 stove at 120 °C for 24 h in air. The residue is hereafter referred to as leached powders.

2.3. Consolidation

Mechanochemically synthesized and leached CeB$_6$ powders were compacted under a uniaxial pressure of 800 MPa in an MSE™ MP-0710 hydraulic press which resulted in cylindrical green compacts with a diameter of 12.7 mm. They were then sintered at 1700 °C for 5 h in a Linn™ HT-1800 high-temperature controlled atmosphere furnace operated at a heating and cooling rate of 10 °C/min under Ar gas at a flow rate of 1000 ml/min. The sintering temperature was selected as 1700 °C in regard to preliminary experiments carried out at temperatures lower than the utilized temperature and reported literature [26,27,30]. According to previous studies, high density CeB$_6$ was obtained after SPS at 1500 °C [26,27]. Since the applied sintering method is pressureless sintering, the samples should be exposed to higher temperature to reach an adequate densification as compared to SPS method.

2.4. Characterization

X-ray diffraction (XRD) investigations of the as-blended, mechanochemically synthesized and leached powders and sintered samples were performed using a Bruker™ D8 Advanced Series X-ray powder diffractometer, with CuK$_\alpha$ (λ = 0.154 nm, 40 kV and 40 mA) radiation in the 2θ range of 10–90° incremented at a step size of 0.02° at a rate of 2°/min. The International Center for Diffraction Data® (ICDD) powder diffraction files were utilized to determine the crystal structure and lattice parameter(s) of the crystalline phases.

The average crystallite sizes and lattice strains of the mechanochemically synthesized CeB$_6$ powders were measured by utilizing Bruker-AXS™ TOPAS V3.0 software based on the modified Scherrer's formula [29]. The

amounts of the different phases in the mechanochemically synthesized CeB$_6$ powders were identified by the semi-quantitative Rietveld method based on the related XRD patterns. General images of the as-blended, mechanochemically synthesized and leached powders were captured by using a Zeiss™ Discovery.V12 stereomicroscope (SM) coupled with a Zeiss™ Axiocam ERc5s high resolution digital camera. Particle size measurements were conducted for the leached powders using a Microtrac™ Nano-flex particle size analyzer (PSA) equipped with a Bandelin Sonopuls™ ultrasonic homogenizer. Thermal properties of the as-blended and mechanochemically synthesized powders were examined using a TA™ Instruments SDT Q600 differential scanning calorimeter (DSC): for each run, 15 mg sample was placed in an alumina crucible and heated up to 1150 °C at a heating rate of 10 °C/min under Ar atmosphere. After DSC analyses, the mechanochemically synthesized and heated powders were subjected to additional XRD analyses to detect the resulting phases. Microstructural characterizations and energy dispersive spectroscopy (EDS) analyses of the mechanochemically synthesized and leached powders were carried out using a Hitachi™ TM-1000 and a FEI™ Quanta FEG 250 scanning electron microscopes (SEM) operated at 15 kV and also using a JEOL™ JEM-2000EX transmission electron microscope (TEM) operated at 160 kV. EDS results were reported as the arithmetic means of three different measurements taken from the same regions in the samples. The powder densities of the final powder products after leaching were measured by a Micromeritics™ AccuPyc II 1340 gas pycnometer in a 1 cm³ sample chamber at room temperature using He gas (Linde™, 99.996% pure) as the displacement medium. Density results of each powder product include the arithmetic mean of ten measurements and standard deviations. The surface areas of the leached powders were determined using a Quantachrome™ Autosorb-IO/MP-XR surface area analyser (SAA) based on the Brunauer-Emmett-Teller (BET) theory. The samples were degassed at 150 °C under N$_2$ gas (Linde™, 99.999% pure) and analysed by N$_2$ absorption at −196 °C using He (for reference) gas. Magnetic properties of the leached powders were measured using a vibrating sample magnetometer (VSM) at room temperature under DC-biased magnetization between 0 and 8000 Oe. Furthermore, the amounts of the elements (B, Mg and Fe) in the supernatant liquid after purification by the leaching process were analysed using a Perkin Elmer™ 1100B atomic absorption spectrometer (AAS).

The density of the sintered sample was measured in ethanol using the Archimedes' method and the results were reported as the arithmetic mean of three different measurements taken from the same sample. To obtain scratch-free mirror finish for electrical resistivity measurements, SEM analyses, Vickers microhardness measurements and sliding wear tests, the sintered samples were subjected to a series of standard

metallographic sample preparation treatments. Electrical resistivity of the polished specimen was measured at room temperature using a four-point probe method in a Signatone™ four-point probe system equipped with a high impedance current source and a voltmeter. The expression for the calculation of electrical resistivity of the bulk structure (ρ) is given elsewhere [30]. Electrical resistivity of the sample includes the arithmetic mean of five measurements carried out at 100–300 mA and the standard deviations.

Vickers microhardness value of the sintered sample was measured using a Shimadzu™ HMV microhardness tester at 100 g load (9.807 N) for 15 s. Microhardness test results for each sample include the arithmetic mean of fifteen successive indentations and standard deviations. Surface roughness value of the sintered sample was measured by using a Veeco™ Dektak 6 M Stylus profilometer under 5 mg applied force for 30 s and with 2 mm length. The sintered sample was subjected to sliding wear test at room temperature in a Tribotechnic™ oscillating tribotester using a 6 mm alumina ball (Tribotechnic™, 99.5% pure) under 4 N applied force, with 2 mm/s sliding speed and 2 mm stroke length for a total sliding distance of 30 000 mm. Wear track of the sintered sample was imaged by the SM and examined by the profilometer. Wear test result in terms of wear volume loss value is the arithmetic mean of five different measurements for each sample.

III. Thermodynamic calculations

Thermodynamic calculations for CeO_2, B_2O_3 and Mg powders were performed using the FactSage™ 6.3 program. The standard Gibbs free energy and enthalpy changes as a function of temperature for Eq. 1 are presented in Fig. 1a and 1b, respectively. According to the plots, Eq. 1 has a large negative standard free energy change (between −2100 and −300 kJ) and standard enthalpy (between −3800 and −2000 kJ) change, which indicates that this reaction is feasible and it can occur spontaneously in the temperature range of 0–2000 °C. As seen in Fig. 1b, the slope of the standard enthalpy-

temperature curve changes at certain temperatures, arising from the melting of B_2O_3 at 450 °C, respective melting and boiling of Mg at 650 °C and 1095 °C and formation of magnesium borate phases until 1100 °C [30]. Additionally, these thermodynamic calculations have revealed that the proposed reduction reaction in Eq. 1 can be spontaneously carried out at room temperature.

Figure 2a shows probable reaction products and their molar amounts as a function of increasing temperature for the CeO_2, B_2O_3 and Mg powders in stoichiometric ratio. According to Fig. 2a, one mole of CeB_6 forms in the presence of 11 mol of MgO up to 1800 °C. Above this temperature, $Mg_3B_2O_6$ forms together with Ce_2O_3, and the amount of CeB_6 phase decreases to 0.5 mol with decreasing MgO amount which is completely consumed at 1900 °C. In addition, Fig. 2b represents variations in the molar amounts of probable reactants and products with increasing molar Mg amount at a constant temperature of 1200 °C. Based on Fig. 2b, it can be stated that by using less than 5 mol of Mg in the initial reactant mixture, some amounts of CeO_2 and B_2O_3 remain in the system together with CeB_6 and $Mg_3B_2O_6$ phases emerging as the reaction products. Besides, by using more than 5 mol of Mg, the molar amounts of CeB_6 and MgO phases increase while the amount of unwanted $Mg_3B_2O_6$ phase decreases. Additionally, for about 11 mol of Mg, the amounts of MgO and CeB_6 reach their maximum and $Mg_3B_2O_6$ completely disappears. However, the possibility of unreacted Mg phase remaining in the system increases above 15 mol of Mg. As clearly seen from Fig. 2b, using stoichiometric amount of Mg (11 mol) results in almost the same amount of CeB_6 phase as with excess usages of Mg.

To explain the reaction mechanism of CeB_6 formation in the CeO_2, B_2O_3 and Mg powders, the thermochemistry of reduction reactions of oxide raw materials with Mg were investigated. Standard Gibbs free energy change versus temperature curves for the reactions given in Eqs. 2, 3 and 4 are displayed in Fig. 3. Standard Gibbs free energy of Eq. 2 changes between −530 and −31 kJ in the temperature range of 0–2000 °C. In addition, Fig. 3 shows that the standard Gibbs free energy of
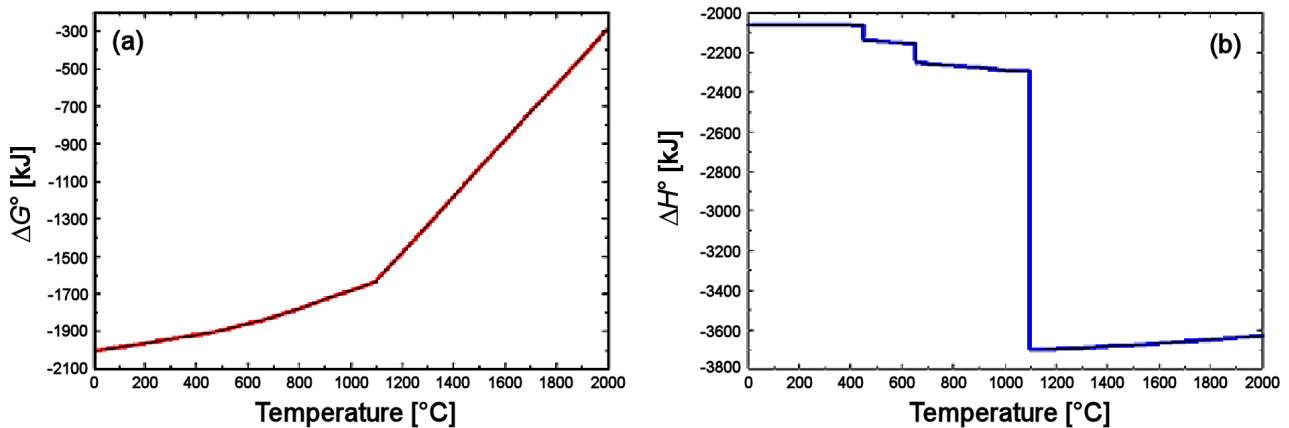

Figure 1. Standard Gibbs free energy change (a) and enthalpy change (b) versus temperature of the reaction in Eq. 1
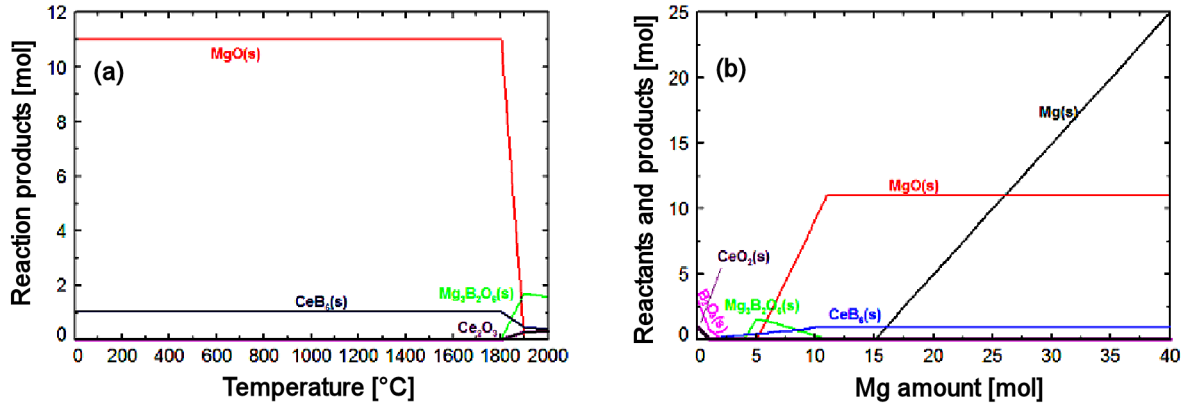
Figure 2. Molar amount of probable products versus temperature (a) and molar amounts of reactants and products versus molar Mg amount (at 1200 °C) (b), based on the reaction in Eq. 1
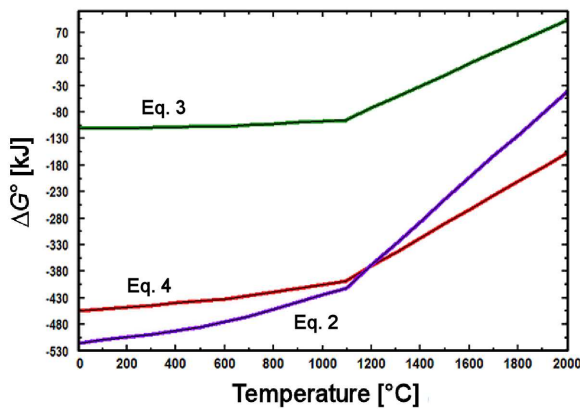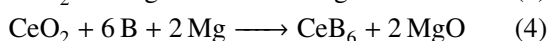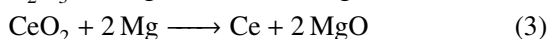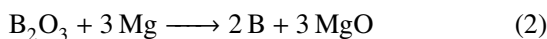

Figure 3. Standard Gibbs free energy change versus temperature curves of the reactions in Eqs. 2, 3 and 4

Eq. 3 varies between −105 and +90 kJ in the same temperature range. Therefore, it can be concluded that the magnesiothermic reduction of B_2O_3 is more favourable than CeO_2 in this temperature range and the overall reaction in Eq. 1 can be thought of as a two-stage reaction in which the first stage is the exothermic reduction of B_2O_3 by Mg. Therefore, it can be interpreted that in the second stage the evolved boron phase comes into contact with CeO_2 particles in the presence of Mg to form CeB_6 as per reaction Eq. 4. The standard free energy change of Eq. 4 with increasing temperature (Fig. 3) shows more negative values (−455 and −155 kJ for 0–2000 °C) than that of Eq. 3. On the basis of these calculations, B_2O_3 and CeO_2 reductions with Mg cannot take place separately as written in Eqs. 2 and 3 during the synthesis. As a result, the reaction mechanism can be explained by an initial reduction of B_2O_3 by Mg and formation of B phase which weakens the atomic bonds between Ce and O and facilitates the transfer of the oxygen atoms from CeO_2 to Mg in regard of Eq. 4.

$$B_2O_3 + 3\,Mg \longrightarrow 2\,B + 3\,MgO \qquad (2)$$
$$CeO_2 + 2\,Mg \longrightarrow Ce + 2\,MgO \qquad (3)$$
$$CeO_2 + 6\,B + 2\,Mg \longrightarrow CeB_6 + 2\,MgO \qquad (4)$$

IV. Results and discussion

4.1. Characterization of CeB_6 powders

Figure 4 illustrates the XRD patterns of the as-blended CeO_2, B_2O_3 and Mg powders and those mechanically milled for different durations up to 5 h. In the XRD pattern of the as-blended (non-milled) powders (Fig. 4a) CeO_2 (ICDD Card No: 81-0792, Bravais lattice: face-centered cubic, $a = 0.541$ nm) and Mg (ICDD Card No: 35-0821, Bravais lattice: primitive hexagonal, $a = 0.329$ nm and $c = 0.521$ nm) phases were detected. The characteristic peaks of B_2O_3 were not detected in the XRD pattern of the as-blended powders due to its amorphous nature. In the XRD patterns of
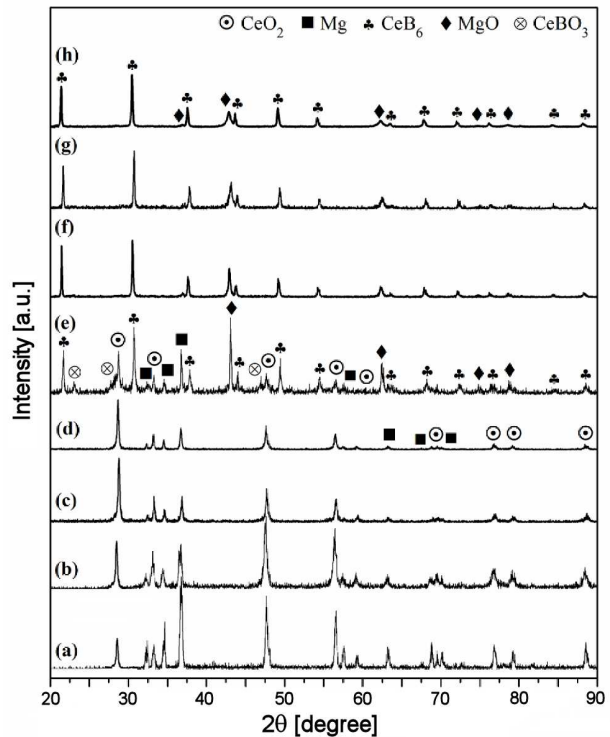

Figure 4. XRD patterns of the CeO_2, B_2O_3 and Mg powders: a) as-blended, and mechanically milled for: b) 1 h, c) 1.5 h, d) 1 h 45 min, e) 2 h, f) 3 h, g) 4 h and h) 5 h

powders milled for 1 h, 1.5 h and 1 h 45 min (in Fig. 4), only CeO_2 and Mg phases are present, indicating that reaction between the initial powders did not start till about 1 h 45 min. Furthermore, the intensities of the CeO_2 and Mg phases decreased with increasing milling time (Fig. 4a-d). This indicates a reduction in the average crystallite sizes of the CeO_2 and Mg powders and hence an increase in their reactivity for the forthcoming reduction reaction. As seen from Fig. 4e, the powders milled for 2 h contain CeO_2, Mg, $CeBO_3$ (ICDD Card No: 21-0177, Bravais lattice: primitive orthorhombic, a = 0.508 nm, b = 0.820 nm, c = 0.581 nm), CeB_6 (ICDD Card No: 38-1455, Bravais lattice: primitive cubic, a = 0.414 nm) and MgO (ICDD Card No: 45-0946, Bravais lattice: face-centered cubic, a = 0.421 nm) phases. Therefore, 2 h milling duration can be considered as the initial point for the formation of the borate and boride phases. At the end of 3 h milling, the only detected phases were CeB_6, $CeBO_3$ and MgO (Fig. 4f). Further milling for 1 h (Fig. 4g) showed the disappearance of $CeBO_3$ which was a transition phase during the formation of CeB_6. Therefore, the reaction in Eq. 1 completely took place after mechanochemical synthesis conducted by milling for 4 h (Fig. 4g). Extending the milling duration to 5 h did not change the nature of the resulting products: CeB_6 and MgO phases were still present in the 5 h milled powders (Fig. 4h) and no new phases were formed. XRD patterns of the CeB_6 phase contained twelve peaks which were consistent with the standard CeB_6 pattern (Fig. 4e-h). The peak intensities of the CeB_6 and MgO phases gradually decreased from 3 to 5 h milling as seen from Fig. 4f-h. On the basis of the related XRD patterns, the average crystallite sizes of the CeB_6 phase in the powders milled for 3, 4 and 5 h were calculated as 178, 149 and 90 nm, respectively.

Stereomicroscope (SM) images of the as-blended and mechanically milled CeO_2, B_2O_3 and Mg powders are shown in Fig. 5. Particle size heterogeneity is clearly observed in Fig. 5a. After milling for 1 h, a homogenous distribution of the particles throughout the microstruc-

ture is enabled (Fig. 5b). The CeO_2, B_2O_3 and Mg powders have a granular and finer morphology after 1.5 h and 1 h 45 min of milling (Figs. 5c,d). When the reaction partially takes place after 2 h of milling, the morphology is converted into an agglomerated form (Fig. 5e) and remains almost unchanged after 3, 4 and 5 h of milling except for reduction in particle size and disappearance of shiny points, probably corresponding to Mg particles (Figs. 5f,g,h).

Figure 6 displays the DSC thermograms of the as-blended CeO_2, B_2O_3 and Mg powders and those mechanically milled for different durations up to 5 h. The DSC curve of the as-blended powders (Fig. 6a) has a very broad endotherm with an onset temperature of 450 °C and a peak point at around 920 °C. This is an overlapping endotherm probably representing the melting of B_2O_3, the melting of Mg and their reaction with CeO_2. DSC curves of the powders milled for 1 h, 1.5 h and 1 h 45 min have the same characteristics with that of the as-blended powder. However, they have three small and shallow exothermic peaks approximately at 600, 650 and 700 °C, probably corresponding to the formation of $CeBO_3$ phase, oxidation of Mg and formation of $Mg_3B_2O_6$ phase, (Fig. 6b-d). The latter two exotherms shift and get smaller in the DSC curve of the 2 h of milled powders (Fig. 6e) because they already contain CeO_2, Mg, $CeBO_3$, CeB_6 and MgO phases after milling. On the other hand, no exothermic peaks are observed in the DSC curves of the powders milled for 3, 4 and 5 h, since they already contain the reaction products of CeB_6 and MgO (Fig. 6f-h).

The XRD patterns of the 1 h, 1 h 45 min, 2 h and 5 h mechanically milled CeO_2, B_2O_3 and Mg powders after DSC analyses up to 1150 °C are shown in Fig. 7. The milled and heated powders contain the same phases: CeB_6, MgO, $Mg_3B_2O_6$ and $CeBO_3$. However, the powder milled for 1 h and 1 h 45 min and heated (Fig. 7a,b) have the dominant $CeBO_3$ phase rather than CeB_6. Thus, additional $CeBO_3$ and $Mg_3B_2O_6$ phases occur instead of yielding only CeB_6 and MgO phases,
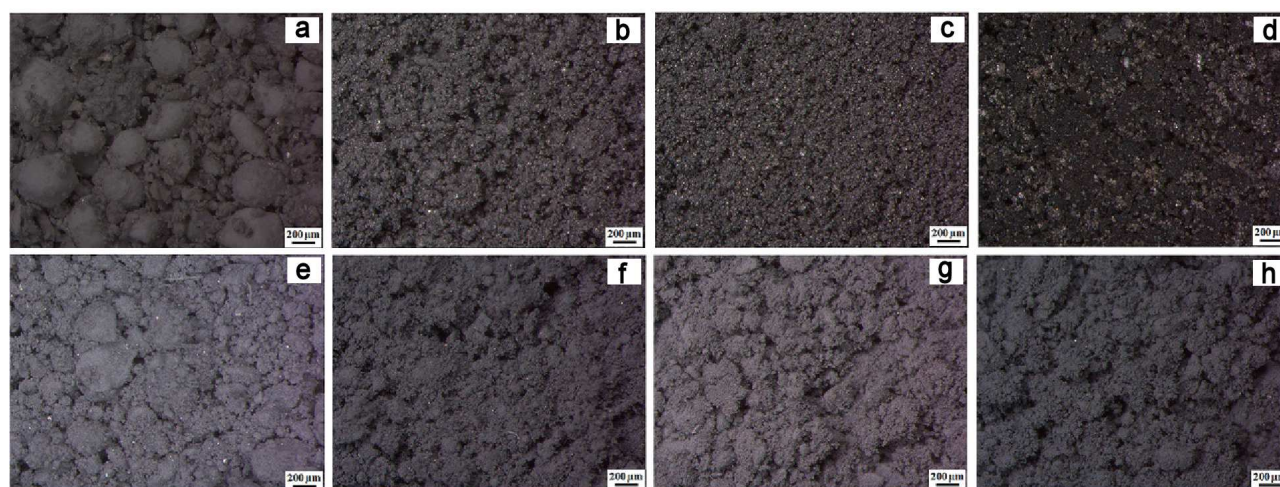

Figure 5. SM images of the CeO_2, B_2O_3 and Mg powders: a) as-blended and mechanically milled for: b) 1 h, c) 1.5 h, d) 1 h 45 min, e) 2 h, f) 3 h, g) 4 h and h) 5 h
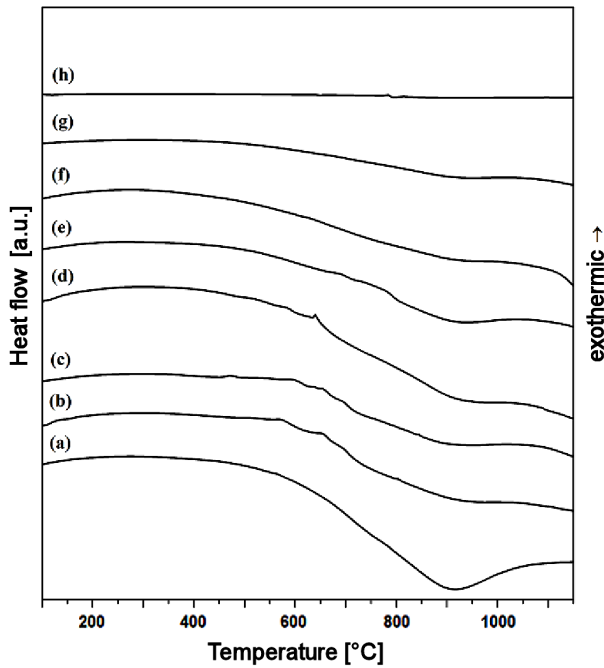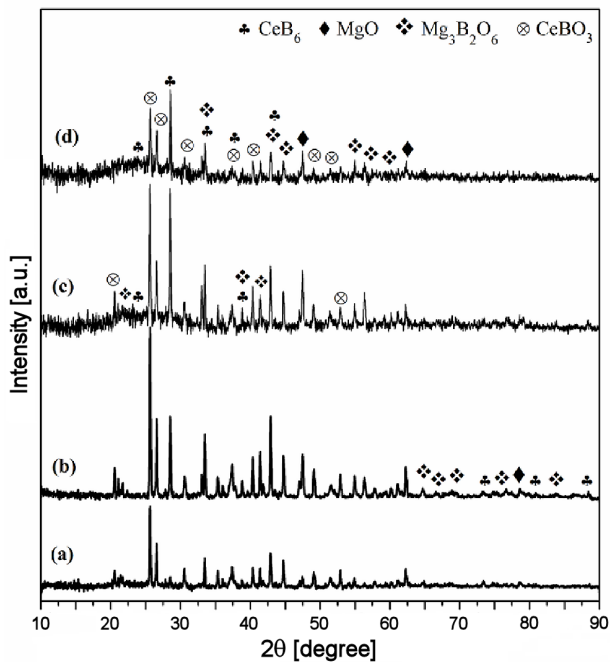
37

Figure 6. DSC thermograms of the CeO_2, B_2O_3 and Mg powders: a) as-blended and mechanically milled for: b) 1 h, c) 1.5 h, d) 1 h 45 min, e) 2 h, f) 3 h, g) 4 h and h) 5 h

Figure 7. XRD patterns of the CeO_2, B_2O_3 and Mg powders mechanically milled at different durations, after DSC analyses up to 1150 °C: a) 1 h, b) 1 h 45 min, c) 2 h and d) 5 h

when a subsequent heat treatment is conducted after milling without the complete reduction reaction. On the other hand, MCS is a one-step process for the formation of CeB_6 phase. Even if 2 h milled powder has the phases of CeO_2, Mg, CeB_6, $CeBO_3$ and MgO together in its structure and 5 h milled powder has the phases of CeB_6 and MgO (Fig. 4e,h), they have similar phases after DSC heating (Fig. 7c,d). CeB_6 is partially converted to

$CeBO_3$ and $Mg_3B_2O_6$ phases during the heating of the 5 h milled powders due to the reaction of some amount of CeB_6 and MgO with each other (Fig. 7d). Similar DSC and following XRD observations were previously reported by Ağaoğulları *et al.* [30] for the Sm_2O_3-B_2O_3-Mg system. On the basis of the XRD and DSC analyses, it is understood that milling duration of 5 h yielded CeB_6 and MgO phases and there exists no exothermic peak corresponding to the oxidation of residual Mg phase. Thus, 5 h was selected as the sufficient MCS time for the latter investigations.

Figure 8 illustrates the XRD pattern of the CeB_6 powders mechanically milled for 5 h and leached with 4 M HCl. As clearly seen, the acid concentration is sufficient to completely remove the MgO phase from the powders. On the other hand, no impurity phases were observed in the XRD pattern within the detection limit of the used diffractometer (>2 wt.%). Moreover, based on the XRD pattern, the average crystallite size of the leached powders was determined as 98 nm. It was reported in a related study that leaching of the CeB_6, MgO and Fe containing MCS products in a 1 M HCl solution for 30 min was sufficient to remove the MgO phase [21]. Although leaching the CeB_6, MgO and $Mg_3B_2O_6$ containing combustion synthesis (CS) products in a 1 M HCl solution for 15 h enabled to eliminate the MgO phase, it was not adequate for the dissolution of $Mg_3B_2O_6$ [21]. In another study, however, MgO and $Mg_3B_2O_6$ phases in CS products were completely removed from CeB_6 powders by leaching with 6 M HCl for more than 4 h under mechanical agitation of 200 rpm at 50 °C [6,31]. Furthermore, HCl concentration of 3 M was earlier accepted as a sufficient leaching concentration to obtain pure (>99%) CeB_6 powders without MgO and $Mg_3B_2O_6$ contaminations [5]. In another related study, the as-synthesized powders containing LaB_6, SmB_6 and CeB_6 phases were purified by applying post treatments such as stirring in 1–6 M HCl so-

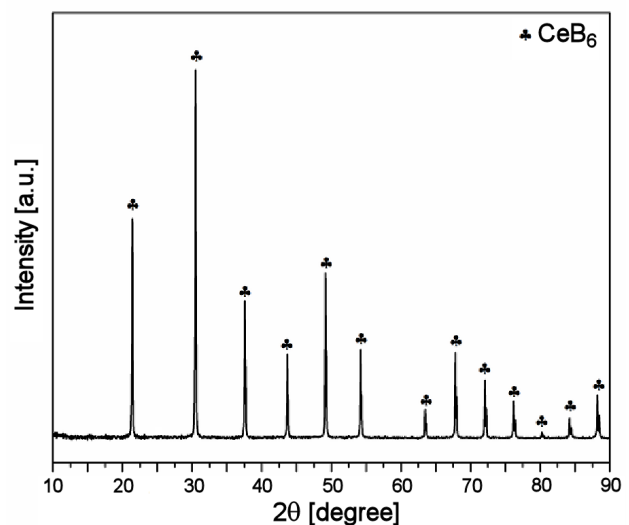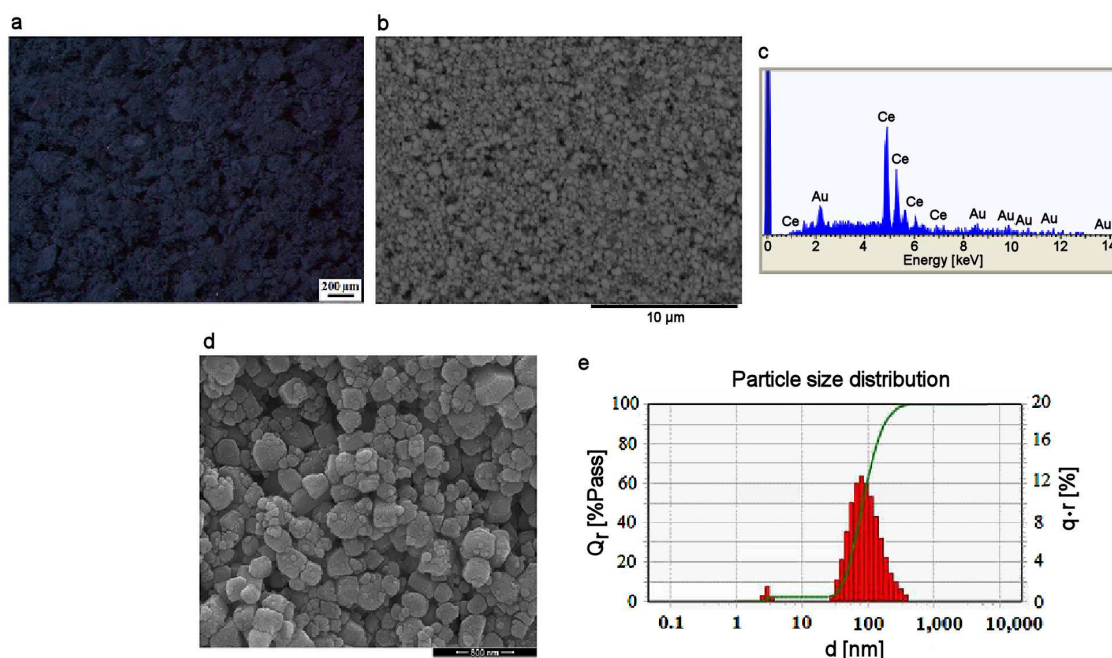**Figure 8. XRD pattern of the CeO_2, B_2O_3 and Mg powders mechanically milled for 5 h and leached with 4 M HCl**

Figure 9. SM (a), low-magnification SEM image (b), general EDS taken from SEM image (c), high-magnification SEM image (d) and PSA image (e) of the CeB$_6$ powders mechanically milled for 5 h and leached with 4 M HCl

lution at 95 °C, filtering, washing and drying [32]. In the present study, AAS analysis was also conducted on the supernatant liquid decanted from leaching treatment of the 5 h milled powders using 4 M HCl; 198 ppm B, 6 ppm Fe and 6563 ppm Mg were determined in the solution. The detection of B and Fe is related with the dissolution of CeB$_6$ because of the highly concentrated HCl acid and dissolution of Fe impurity released from the milling media, respectively. Repeated HCl leaching was also carried out, and Fe and Mg were found as trace amounts in the supernatant liquid. Thus, it can be stated that the leached powders have sufficient purity without the presence of any impurity soluble in HCl acid.

Figure 9a displays the SM image of the CeB$_6$ powders obtained after milling for 5 h and leaching with 4 M HCl. As compared to the SM image of the 5 h milled powders in Fig. 5h, it can be seen that MgO was completely removed and the bluish-violet colour of the CeB$_6$ powders appeared after the leaching treatment. The leached CeB$_6$ powders have round-shaped particles (SEM image, Fig. 9b). The general EDS measurement (Fig. 9c) taken from the area in this image reveals the presence of Ce and Au (from the coating) elements, indicating that only CeB$_6$ particles are present in the microstructure without any detection of impurity element. The SEM image at a higher magnification in Fig. 9d shows the CeB$_6$ particles ranging in size between 50 and 150 nm. In addition, the PSA graph (Fig. 9e) indicates that the average particle size of the CeB$_6$ is about 86 nm which is in the range observed in the SEM image in Fig. 9d.

Figure 10 illustrates the TEM/EDS images of the CeB$_6$ powders mechanically milled for 5 h and leached with 4 M HCl. Figure 10a is a BF image showing

equiaxed particles varying in sizes between 75 and 100 nm. Figure 10b is the corresponding SADP image of the white-circled region marked in this BF image; the sharp and continuous rings suggest the presence of fine CeB$_6$ particles. Figure 10c is another BF image representing the irregular-shaped particles in size range of 50–150 nm. The general EDS measurement (Fig. 10d) taken on this BF image reveals that the pow-
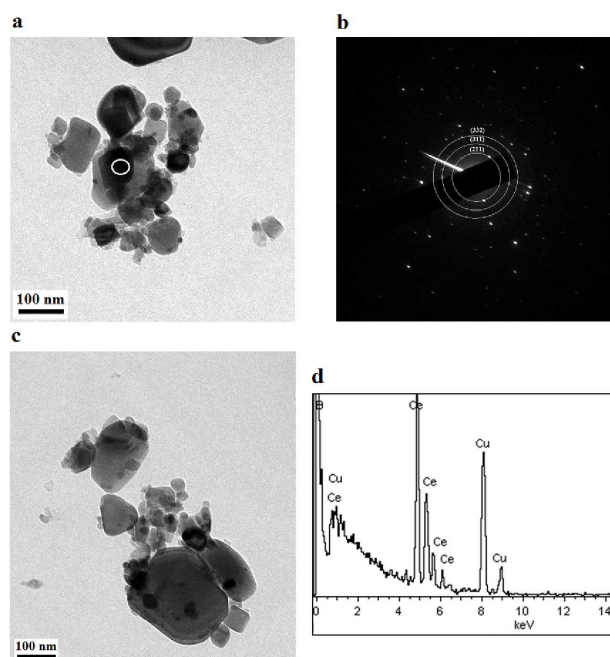
Figure 10. TEM images of the CeB$_6$ powders mechanically milled for 5 h and leached with 4 M HCl: a) BF image, b) its SADP taken from the white-circled region revealing CeB$_6$ phase, c) another BF image and d) its general EDS analysis (objective aperture is on (001) and camera length is 100 cm)

ders have composition with 71.79 ± 0.93 wt.% Ce and 28.21 ± 0.36 wt.% B, which is close to their stoichiometric amounts in CeB_6 phase (Ce: 68.36 wt.% and B: 31.64 wt.%).

The density value of the synthesized CeB_6 powders after milling and leaching was determined by He gas pycnometer as 4.77 ± 0.009 g/cm^3, which is close to its theoretical density value of 4.79 g/cm^3. Additionally, the surface area value of the synthesized CeB_6 powders was determined as 13.45 m^2/g. This indicates that the particle size of CeB_6 is in nanoscale (86 nm). Additionally, Fig. 11 represents the magnetic measurement of the synthesized CeB_6 powders at room temperature and confirms its tendency to be paramagnetic. As previously reported in the literature, rare-earth hexaborides display a remarkable variation in their magnetic properties [33]. There are diamagnetic, Pauli-paramagnetic, ferromagnetic, anti-ferromagnetic and more complex spin-ordered hexaborides reported in the literature [33]. Most of the magnetic properties are considered very sensitive to the number of valence electrons available in the valence band. In other words, the magnetic properties of the rare-earth hexaborides strongly depend on stoichiometry (rare-earth metal/B ratio), impurity and homogeneity ranges. Thus, there are inconsistencies among the numerous reported magnetic investigations of rare-earth hexaborides due to the differences in composition arising from the method of preparation [33]. Consequently, it can be inferred from the magnetic measurements that the synthesized CeB_6 powders do not include any Fe contamination since they do not exhibit a ferromagnetic tendency (Fig. 11).

4.2. Consolidation and bulk properties of CeB$_6$

The XRD pattern of the sintered specimen obtained from the pure CeB_6 powders prepared via milling for 5 h and leaching with 4 M HCl is shown in Fig. 12. The XRD pattern shows that the bulk sample has only the CeB_6 phase. There is no new phase formation at high-
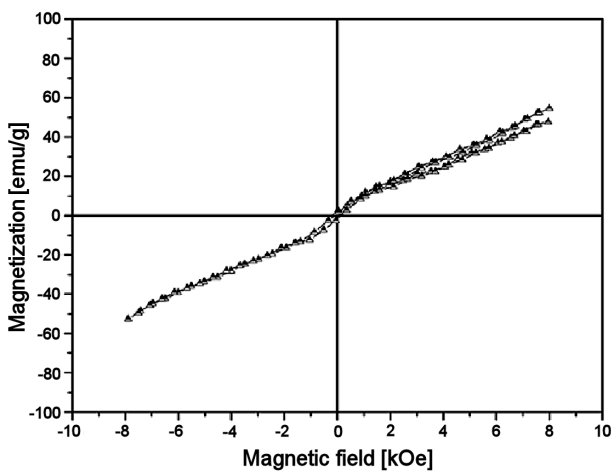
temperature or contamination resulting from the sintering process by the effect of high temperature. Thus, XRD pattern of the sintered sample (Fig. 12) is very similar to that of the leached powder (Fig. 8). However, the average crystallite size of the bulk sample calculated from the XRD is slightly higher (115 nm) as compared to the leached powder (98 nm) due to the effect of temperature. Table 1 lists some physical and mechanical properties of this bulk CeB_6 sample. As seen from Table 1, the density of the sintered sample was determined as 4.56 g/cm^3, accordingly the relative density was calculated as 95.20% TD. Bao *et al.* [16] reported that nano (ball-milled) and coarse powders of CeB_6 spark plasma sintered at 1550 °C at a pressure of 50 MPa had the relative density of 99.1 and 76.7% TD, respectively. In an earlier study related to the conventional hot pressing of rare-earth hexaborides, the sintering temperature and the relative density were respectively reported as 1900 °C and 90% TD, indicating that this method is not sufficient to obtain full densification [16]. A higher relative densification rate was achieved in this study when compared with the reported study. It is most likely due to the nanocrystalline structure and high purity of the synthesized powders which contribute to accelerated densification.

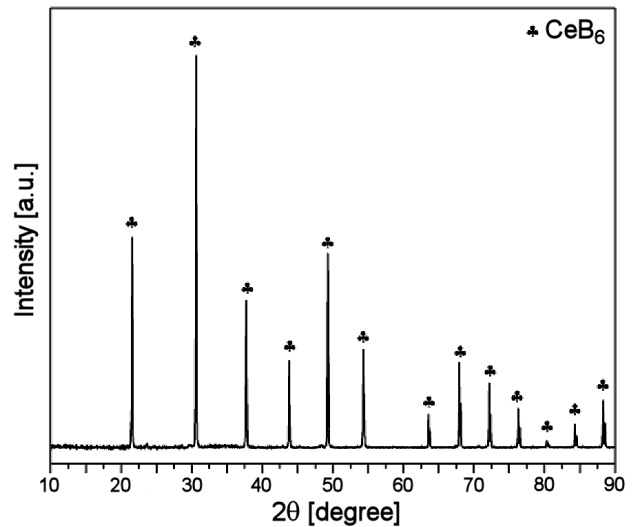Furthermore, the electrical resistivity of bulk CeB_6

Figure 12. XRD pattern of the sintered CeB$_6$ sample

Table 1. Some properties of the sintered CeB$_6$ bulk derived from the CeB$_6$ powders mechanically milled for 5 h and leached with 4 M HCl

Properties	Bulk CeB$_6$
Archimedes density [g/cm^3]	4.56
Relative density [% TD]	95.2
Electrical resistivity [μΩ·cm]	57.50 ± 3.80
Microhardness [GPa]	11.65 ± 0.50
Mean surface roughness [μm]	0.605
Mean friction coefficient	0.33
Wear rate [mm^3/N·m]	1.46×10^{-4}

Figure 11. Magnetic field versus magnetization curve of the CeB$_6$ powders mechanically milled for 5 h and leached with 4 M HCl

was measured as 57.50 ± 3.80 μΩ·cm. Weimer [4] reported the electrical resistivity values of some borides: CrB (45.5 μΩ·cm), CrB_2 (30 μΩ·cm), HfB_2 (10.6 μΩ·cm), NbB_2 (25.7 μΩ·cm), TaB_2 (32.5 μΩ·cm), TiB_2 (9 μΩ·cm), VB (35 μΩ·cm), VB_2 (22.7 μΩ·cm) and ZrB_2 (9.7 μΩ·cm). Additionally, the electrical resistivity of bulk SmB_6 was previously reported as ~211 μΩ·cm [30]. Therefore, it can be stated that CeB_6 exhibits an electrical resistivity value similar to other boride compounds excluding IVB diborides (TiB_2, ZrB_2 and HfB_2). Lundström [33] reported that the rare-earth hexaborides exhibit significant variations in terms of electrical properties. Most of the electrical properties are very sensitive to the number of valence electrons available in the valence band and depend on the stoichiometry, impurity and homogeneity ranges of the borides. Moreover, the electrical resistivities of the rare-earth hexaborides may differ because of the differences in composition arising from the synthesis method [32–34]. For example, the resistivity of the CeB_6 crystals obtained by the flux method was higher than that obtained by the floating zone method due to the deviation from the stoichiometry, presence of uncontrolled Al impurity, and higher oxygen content [35,36]. Also, the electrical resistivity of bulk CeB_6 prepared by the SPS method increased from 36.34 to 60.54 μΩ·cm with increasing temperature from 25 to 500 °C, indicating a metallic conducting behaviour [16]. Furthermore, CeB_6 has approximately 20 μΩ·cm higher electrical resistivity than that of LaB_6 in the temperature range of 25–500 °C pointing out its suitability as a more appropriate direct heating cathode [16].

As seen from Table 1, the microhardness value of the bulk CeB_6 was determined as 11.65 ± 0.50 GPa. In a related study carried out on rare-earth hexaborides, the hardness of CeB_6 crystals prepared by travelling solvent floating zone method using oxides and boron powders was found to be 1090 kg/mm^2 [36]. Polycrystalline bulk CeB_6 cathode fabricated by the SPS method using optimum process parameters (1500 °C, 50 MPa and 5 min) had a relative density of 99.61% TD and a hardness value of 2051 kg/mm^2 [27]. In another study, the hardness value of bulk CeB_6 sample was reported as 2550 HV$_{50}$ [22]. Vickers hardness values of the CeB_6 bulks sintered from nanoscale and coarse powders by SPS (at 1550 °C and 50 MPa) were respectively found to be 2160 and 1435 kg/mm^2 and the difference was attributed to the finer particle size and more homogeneous microstructure provided by the usage of nanopowders [16]. Thus, the hardness values for CeB_6 can differ significantly from one sample to another since the hardness strongly depends on the powder properties (influenced by the synthesis method) and consolidation techniques. In addition, the surface roughness and friction coefficient of CeB_6 were determined as 0.605 μm and 0.33, respectively. It was reported that the surfaces of the CeB_6 crystals grown by flux and floating zone methods are considerably different. The roughness amplitudes of

the samples obtained by the floating zone method are higher than those obtained by the flux method [35].

After dry sliding wear test of bulk CeB_6, wear width and depth of 709 and 15.75 μm, wear area of 8765.89 μm^2 and wear volume loss of 0.0175 mm^3 were recorded. Accordingly, the wear rate of bulk CeB_6 was calculated as 1.46×10^{-4} mm^3/N·m indicating a high wear resistance. A similar wear rate value was reported previously by Ağaoğulları *et al.* [30] for the bulk SmB_6 as 1.61×10^{-4} mm^3/N·m. Figure 13a shows the SM image taken from the surface of the bulk CeB_6 after sliding wear test, and Fig. 13b illustrates the OM image of the contact surface of the sliding Al_2O_3 ball used during the wear test. The general image in Fig. 13a shows a shallow wear track on the surface which conforms well with the measured wear width and area values. Therefore, it can be said that CeB_6 shows a high wear resistance under the utilized test conditions by virtue of its high densification rate and high hardness. Furthermore, the worn and flattened surface of the Al_2O_3 ball in Fig. 13b indicates a mutual wear between the bulk CeB_6 and Al_2O_3 ball although Al_2O_3 has a higher hardness. This wear behaviour can be accepted as an indication of high hardness and wear resistance of CeB_6 (Table 1).
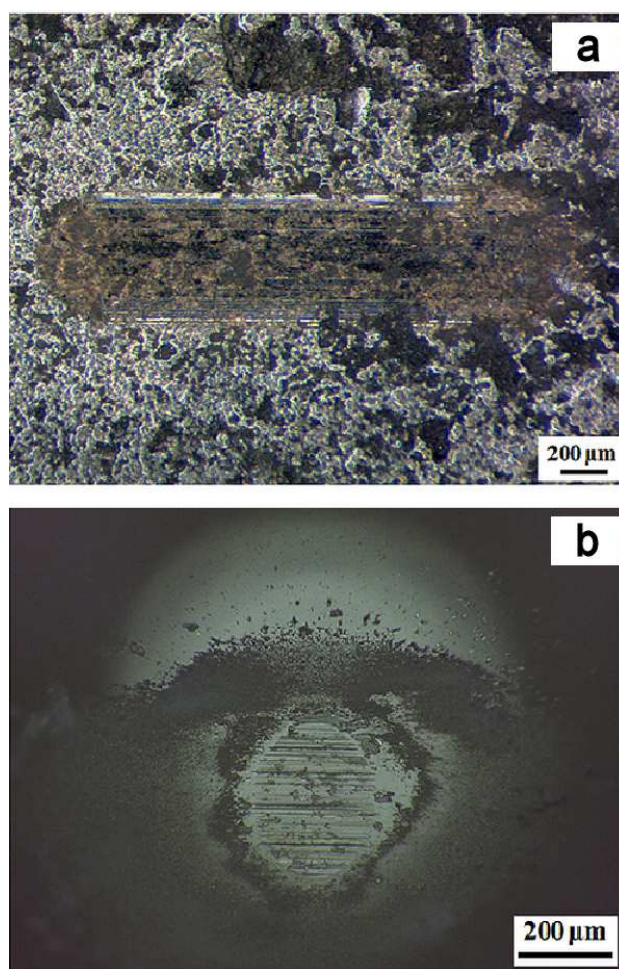
Figure 13. Wear track SM image (a) of the bulk CeB_6 sample, and worn surface OM image (b) of the alumina ball sliding on the surface of bulk CeB_6

Thus, nanostructured CeB_6 powders of high-purity were prepared via a facile synthesis route consisting of room temperature mechanochemical synthesis in a high-energy ball mill (5 h of milling) and a subsequent purification process (leaching with 4 M HCl). Additionally, the bulk CeB_6 sample prepared by cold pressing and pressureless sintering showed high densification rate. Its physical and mechanical properties were improved thanks to the characteristics of CeB_6 powders. Thus, the processing techniques described in this study can be proposed as simple and economical routes for preparing nanostructured rare-earth hexaborides.

V. Conclusions

In the present study, nanostructured bulk CeB_6 was successfully prepared through three steps including mechanochemical synthesis, purification by HCl leaching, and cold-pressing/pressureless sintering. The results of this study can be summarized as follows:

- The formation mechanism of CeB_6 was explained by thermodynamic calculations using FactSage software. Based on the thermodynamical investigations, the formation reaction of CeB_6 included different steps as follows: The reduction of B_2O_3 by Mg and the reaction of CeO_2 and Mg in the presence of B and the formation of CeB_6 and MgO.
- During the mechanochemical processing of CeO_2, B_2O_3 and Mg starting powders, formation of the CeB_6 phase started only after 2 h of milling together with CeO_2, Mg, MgO and $CeBO_3$ phases.
- Extending the milling duration to 5 h resulted in the disappearance of the borate phases yielding only CeB_6 and MgO.
- Powders milled for 5 h were successfully purified by leaching in 4 M HCl resulting in the formation of high-purity CeB_6 powders free from undesired MgO.
- The purified CeB_6 powders exhibited rounded-shape morphology and had an average particle size of 86 nm.
- CeB_6 powders were consolidated by cold pressing and pressureless sintering at 1700 °C for 5 h and densified up to 95.2% TD which is a comparatively high relative density, attributed mainly to the nanostructured and highly pure powder characteristics.
- Bulk CeB_6 had paramagnetic tendency and electrical resistivity value of ~57.50 μΩ·cm.
- The bulk CeB_6 had a hardness value of ~11.65 GPa and a wear rate of 1.46×10^{-4} mm³/N·m indicating a relatively high wear resistance.

References

1. X.H. Ji, Q.Y. Zhang, J.Q. Xu, Y.M. Zhao, "Rare-earth hexaborides nanostructures: recent advances in materials, characterization and investigations of physical properties", *Prog. Solid State Chem.*, **39** (2011) 52–69.
2. R.K. Selvan, I. Genish, I. Perelshtein, M.C. Moreno, A. Gedanken, "Single step, low-temperature synthesis of submicron-sized rare earth hexaborides", *J. Phys. Chem. C*, **112** (2008) 1795–1802.
3. L.W. Swanson, D.R. McNeely, "Work functions of the (001) face of the hexaborides of Ba, La, Ce and Sm", *Surf. Sci.*, **83** (1979) 11–28.
4. L. Wang, L. Xu, Z. Ju, Y. Qian, "A versatile route for the convenient synthesis of rare-earth and alkaline-earth hexaborides at mild temperatures", *Cryst. Eng. Comm.*, **12** (2010) 3923–3928.
5. C. Fu, J. Xu, Y. Chang, Q. Wang, Y. Wang, B. Yu, P. Guo, J. Xu, H. Sun, Y. Luo, J. Liu, "Flexible three dimensional CeB_6 nanowire arrays, and excellent field emission emitters", *J. Alloy. Compd.*, **729** (2017) 997-1003.
6. J. K. Sonber, T.S.R. Ch. Murthy, K. Sairam, B. Paul, J.K. Chakravartty, "Effect of $TiSi_2$ addition on densification of cerium hexaboride", *Ceram Int.*, **42** (2016) 891–896.
7. C.Y. Zou, Y.M. Zhao, J.Q. Xu, "Synthesis of single-crystalline CeB_6 nanowires", *J. Cryst. Growth*, **291** (2006) 112–116.
8. H. Zhang, Q. Zhang, J. Tang, L.C. Qin, "Single-crystalline CeB_6 nanowires", *J. Am. Chem. Soc.*, **127** (2005) 8002–8003.
9. M. Zhang, X. Wang, X. Zhang, P. Wang, S. Xiong, L. Shi, Y. Qian, "Direct low-temperature synthesis of RB_6 (R = Ce, Pr, Nd) nanocubes and nanoparticles", *J. Solid State Chem.*, **182** (2009) 3098–3104.
10. A. Aprea, A. Maspero, N. Masciocchi, A. Guagliardi, A.F. Albisetti, G. Giunchi, "Nanosized rare-earth hexaborides: low-temperature preparation and microstructural analysis", *Solid State Sci.*, **21** (2013) 32–36.
11. K. Amalajyothi, L.J. Berchmans, A. Visuvasam, S. Angappan, "Electrosynthesis of cerium hexaboride using lithium tetra borate melt", *Mater. Manuf. Proces.*, **26** (2011) 792–795.
12. K. Amalajyothi, L.J. Berchmans, S. Angappan, A. Visuvasam, "Electrosynthesis of cerium hexaboride by the molten salt technique", *J. Cryst. Growth*, **310** (2008) 3376–3379.
13. M. Jha, R. Patra, S. Ghosh, A.K. Ganguli, "Vertically aligned cerium hexaboride nanorods with enhanced field emission properties", *J. Mater. Chem.*, **22** (2012) 6356–6366.
14. Z. Dou, T. Zhang, Y. Guo, J. He, "Research on preparation optimization of nano CeB_6 powder and its high temperature stability", *J. Rare Earths*, **30** (2012) 1129–1133.
15. Y. Tanaka, U. Staub, Y. Narumi, K. Katsumata, V. Scagnoli, S. Shimomura, Y. Tabata, Y. Onuki, "Non-

resonant X-ray Bragg diffraction by CeB$_6$", *Physica B: Condens. Matter*, **345** (2004) 78–81.

16. T.S.R.Ch. Murthy, J.K. Sonber, K. Sairam, R.D. Bedse, J.K. Chakravartty, "Development of refractory and rare earth metal borides & carbides for high temperature applications", *Mater. Today Proc.*, **3** (2016) 3104–3113.

17. G. Bliznakov, P. Peshev, "The preparation of cerium, praseodymium, and neodymium hexaborides", *J. Less Common Met.*, **7** (1964) 441–446.

18. G.V. Samsonov, Yu.B. Paderno, V.S. Fomenko, "Hexaborides of the rare-earth metals", *Sov. Powder Metall. Metal Ceram.*, **2** (1963) 449–454.

19. A. Iltis, P. Maestro, "Rare earth boride abrasive/polishing agents". *US patent 4936875A* (June, 1990).

20. Z. Dou, T. Zhang, Y. Liu, Y. Guo, J. He, "Preparation of CeB6 nano-powders by self-propagating high-temperature synthesis (SHS)", *J. Rare Earths*, **29** (2011) 986–990.

21. B. Akgun, N. Sevinc, H.E. Camurlu, Y. Topkaya, "Mechanochemical and combustion synthesis of CeB$_6$", *Int. J. Mater. Res.*, **104** (2013) 403–407.

22. C. Mitterer, W. Waldhauser, U. Beck, G. Reiners, "Structure and properties of decorative rare-earth hexaboride coatings", *Surf. Coat. Technol.*, **86-87** (1996) 715–721.

23. J.Q. Xu, T. Mori, Y. Bando, D. Golberg, D. Berthebaud, A. Prytuliak, "Synthesis of CeB$_6$ thin films by physical vapor deposition and their field emission investigations", *Mater. Sci. Eng. B*, **177** (2012) 177–120.

24. A. Iltis, P. Maestro, "Preparation of rare earth borides". *US Patent 4999176A* (March, 1991).

25. A. Iltis, P. Maestro, "Preparation of rare earth borides". *US Patent 5176890A* (January, 1993).

26. L. Bao, J. Zhang, S. Zhou, "Effect of particle size on the polycrystalline CeB$_6$ cathode prepared by spark plasma sintering", *J. Rare Earths*, **29** (2011) 580–584.

27. S. Zhou, J. Zhang, D. Liu, L. Bao, "Properties of CeB$_6$ cathode fabricated by spark plasma reactive liquid phase sintering method", *J. Inorg. Mater.*, **24** (2009) 793–797.

28. C. Suryanarayana, "Mechanical alloying and milling", *Prog. Mater. Sci.*, **46** (2001) 1–184.

29. C. Suryanarayana, M.G. Norton, *X-Ray Diffraction: A Practical Approach*, Plenum Press, New York 1998.

30. D. Ağaoğulları, Ö. Balcı, M.L. Öveçoğlu, C. Suryanarayana, İ. Duman, "Synthesis of bulk nanocrystalline samarium hexaborides", *J. Eur. Ceram. Soc.*, **35** (2015) 4121–4136.

31. Z. Dou, T.A. Zhang, J.C. He, "Preparation and characterization of cerium hexaboride nanometer powders by combustion synthesis", *Adv. Mater. Res.*, **236** (2011) 1670–1674.

32. Y. Qian, L. Xu, X. Ma, L. Wang, "Method for preparing nano superfine rare-earth hexaboride powder". *Chinese Patent 101948117A* (January, 2011).

33. T. Lundström, "Structure, defects and properties of some refractory borides", *Pure Appl. Chem.*, **57** (1985) 1383–1390.

34. I. Binder, "Structure and properties of rare-earth and yttrium hard metals", *J. Am. Ceram. Soc.*, **43** (1960) 287–292.

35. V. Petrosyan, V. Vardanyan, V. Kuzanyan, M. Konovalov, V. Gurin, A. Kuzanyan, "Thermoelectric properties and chemical composition of CeB$_6$ crystals obtained by various methods", *Solid State Sci.*, **14** (2012) 1653–1655.

36. S. Otani, H. Nakagawa, Y. Nishi, N. Kieda, "Floating zone growth and high temperature hardness of rare-earth hexaboride crystals: LaB$_6$, CeB$_6$, PrB$_6$, NdB$_6$, and SmB$_6$", *J. Solid State Chem.*, **154** (2000) 238–241.